

# The Planetary Luminosity Problem: “Missing Planets” and the Observational Consequences of Episodic Accretion

SEAN D. BRITTAIN,<sup>1,\*</sup> JOAN R. NAJITA,<sup>2</sup> RUOBING DONG,<sup>3</sup> AND ZHAOHUAN ZHU<sup>4</sup>

<sup>1</sup>*Clemson University*

*118 Kinard Laboratory Clemson, SC 29634, USA*

<sup>2</sup>*National Optical Astronomical Observatory*

*950 North Cherry Avenue*

*Tucson, AZ 85719, USA*

<sup>3</sup>*Department of Physics & Astronomy*

*University of Victoria*

*Victoria BC V8P 1A1, Canada*

<sup>4</sup>*Department of Physics and Astronomy*

*University of Nevada, Las Vegas*

*4505 S. Maryland Pkwy.*

*Las Vegas, NV 89154, USA*

(Received February 28, 2022; Revised TBD; Accepted TBD)

Submitted to ApJ

## ABSTRACT

The high occurrence rates of spiral arms and large central clearings in protoplanetary disks, if interpreted as signposts of giant planets, indicate that gas giants form commonly as companions to young stars ( $< \text{few Myr}$ ) at orbital separations of 10–300 au. However, attempts to directly image this giant planet population as companions to more mature stars ( $> 10 \text{ Myr}$ ) have yielded few successes. This discrepancy could be explained if most giant planets form “cold start,” i.e., by radiating away much of their formation energy as they assemble their mass, rendering them faint enough to elude detection at later times. In that case, giant planets should be bright at early times, during their accretion phase, and yet forming planets are detected only rarely through direct imaging techniques. Here we explore the possibility that the low detection rate of accreting planets is the result of episodic accretion through a circumplanetary disk. We also explore the possibility that the companion orbiting the Herbig Ae star HD 142527 may be a giant planet undergoing such an accretion outburst.

*Keywords:* stars: individual (HD 142527) — planets and satellites: formation — protoplanetary disks — planet–disk interactions — planets and satellites: detection

## 1. INTRODUCTION

Giant planets are common at small orbital separations, as are indirect signatures of their existence at large separations. At orbital separations  $\lesssim 10 \text{ au}$ , 10–20% of low mass stars ( $< 1.5 M_{\odot}$ ; LMS), host a gas giant planet ( $\gtrsim 1 M_J$ ; Cassan et al. 2012; Cumming et al. 2008). At large separations ( $\gtrsim 10 \text{ au}$ ), a high occurrence rate of giant planetary companions to LMS is also inferred, based

on the morphologies of protoplanetary disks surrounding young LMS (i.e., T Tauri stars). Some 10–15% of T Tauri disks have the spectral energy distribution (SED) of a transition disk, i.e., a protoplanetary disk in which the central portion ( $\lesssim 10\text{--}40 \text{ au}$ ) is optically thin in the infrared continuum (Muzerolle et al. 2010a). Transition disk morphologies and other corroborating properties are interpreted as the signpost of one or more giant planets ( $\gtrsim 3 M_J$ ) orbiting within the optically thin region of the disk (Dodson-Robinson & Salyk 2011; Zhu et al. 2011; Espaillat et al. 2014a).

A similar story is found for giant planet companions to intermediate mass stars ( $\sim 1.5\text{--}2 M_{\odot}$ ; IMS). At small or-

Corresponding author: Sean D. Brittain  
sbritt@clemson.edu

\* Visiting Scientist, NOAO

bital separations, radial velocity studies find that  $\sim 14\%$  of IMS harbor a gas giant planet within  $\sim 10$  au of the star (Luhn et al. 2018; Johnson et al. 2010). Transition disk SEDs are also common among young IMS (i.e., Herbig Ae stars); approximately 40% of Herbig Ae stars within 200 pc are transition disk sources Brittain & Najita (2019). In addition, a surprisingly large fraction of well-studied Herbig Ae disks show dramatic two-arm spirals ( $\sim 20\%$  Dong et al. 2018a), which point to the presence of high mass giant planets ( $5\text{--}13 M_J$ ) at 30–300 au (Fung & Dong 2015; Dong & Fung 2017).

In contrast to the high frequency of indirect indicators of giant planets beyond  $\sim 10$  au, direct detection of the planets themselves has proven challenging as companions to both mature stars as well as young stars surrounded by protoplanetary disks. Many high contrast imaging surveys have searched for giant planet companions to stars older than 10 Myr at orbital separations  $> 10$  au. As summarized by Bowler (2016, see also Nielsen et al. 2019), such studies find that high mass planets ( $5\text{--}13 M_J$ ) are detected at 30–300 au orbital separation in only a small fraction of mature IMS (2.8% Bowler 2016), assuming they are as bright as predicted by “hot start” planetary evolutionary models. The low incidence rate is much less than the  $\sim 20\%$  two-arm spiral arm fraction of young IMS that points to planets in the same range of mass and orbital separation (Dong et al. 2018a). For mature LMS stars,  $\sim 1\%$  have a  $1\text{--}13 M_J$  giant planet at 10–100 au (Nielsen et al. 2019, Figure 18), a much lower occurrence rate than the 10–15% occurrence rate of transition disks among the T Tauri star population.

The discrepancy between the detection rates of indirect signposts of planet formation and of the planets themselves could indicate that the indirect signposts are caused by something other than planets. For example, two-armed spirals can also arise from gravitationally unstable disks (Dong et al. 2015a; Kratter & Lodato 2016). However, the lifetime of the gravitationally unstable phase is too short to account for the large number of two-armed spirals observed around young stars (Dong et al. 2018a; Hall et al. 2018).

Alternatively, the discrepantly low detection rate of high mass giant planets as companions to mature stars could be entirely due to the use of the hot start models, which assume that planets retain their heat of formation (i.e., gravitational potential energy) when they form. The alternative “cold start” models (Marley et al. 2007; Fortney et al. 2008) assume that planets radiate away much of their accretion energy in the formation phase. As a result, they predict considerably fainter planets at ages  $> 10$  Myr compared to hot start models.

Stone et al. (2018) found that essentially all nearby FGK stars could harbor one or more  $7\text{--}10 M_J$  planets at 5–50 au if they formed cold start. The planets are simply too faint to be detected with current surveys.

While the above discrepancy could point to the validity of cold start models over hot start models, that scenario implies that accreting planets would be very bright in their youth as they radiate away their accretion energy in accretion shocks and/or through a circumplanetary disk. That is, young giant planets ( $< \text{few Myr}$ ) embedded in protoplanetary disks should be readily detectable during their runaway accretion phase (Eisner 2015; Zhu 2015).

So it is perhaps surprising that giant planets are detected infrequently as companions to young stars surrounded by protoplanetary disks. While transition disks have been targeted in many high contrast imaging studies (e.g., Subaru SEEDS), planetary companion candidates have been detected in only a few sources. The best candidates to date are the companions to two LMS transition disks—PDS 70 (Keppler et al. 2018) and LkCa 15 (Kraus & Ireland 2012; Sallum et al. 2015)—and the companions to the IMS transition disk HD 100546 (Pérez et al. 2019; Brittain et al. 2019). As in the case of the spatially resolved (stellar) companion to the IMS transition disk HD 142527 (Biller et al. 2012; Close et al. 2014), H $\alpha$  emission from the PDS 70 and LkCa 15 companions suggests that they are actively accreting.

Here we explore the reason for the infrequent detection of accreting giant planets in protoplanetary disks despite the likelihood that such planets occur commonly and radiate away their accretion energy as they accrete. We propose that the low “luminosity problem” of forming planets is solved in a similar fashion to the luminosity problem of forming stars (Kenyon et al. 1990; Kenyon & Hartmann 1995). Namely, forming planets accrete episodically, much like how forming stars undergo FU Ori-like outbursts. Previous studies have argued that circumplanetary disks, like circumstellar disks, are likely to harbor significant dead zones and would accrete episodically (Lubow & Martin 2012), or that vortices form in circumplanetary disks and generate short-timescale outbursts (Zhu et al. 2016).

To explore this scenario in the context of the developing detection statistics and properties of young planetary companions, we summarize in section 2 the properties of resolved planetary companions to young protoplanetary disk sources. In section 3, we describe a simple toy model for episodic accretion based on the theoretical literature and illustrate how episodic accretion can potentially account for the low detection rate of accreting

planets. In section 4, we explore the possibility that the companion to HD 142527 is actually a planetary companion undergoing an accretion outburst rather than a low mass stellar companion and discuss ways to discriminate between the two possibilities. We conclude with a discussion of our results and opportunities for future progress.

## 2. SEARCHES FOR YOUNG PLANETS

The largest published near infrared imaging survey for planets forming in protoplanetary disks was carried out in the SEEDS campaign using Subaru/HiCIAO. Uyama et al. (2017) reported SEEDS observations of 68 YSOs (39 LMS and 29 IMS) at NIR wavelengths. Some of the targets were primarily observed in polarization differential imaging mode to probe disk structures, while a fraction of the targets were observed in angular differential imaging (ADI) mode under decent conditions. Specifically, for 20 targets a 5- $\sigma$  contrast level of 5 magnitudes or more was achieved at  $H$ -band at  $0''.25$  separation, which corresponds to a typical upper limit on a planet's  $H$ -band luminosity of  $3 \times 10^{31} \text{ erg s}^{-1} \mu\text{m}^{-1}$  (Table 1) and a planet mass limit of 5-10  $M_J$  at a few tens of AU, assuming hot start models (Baraffe et al. 2003). These results are based on conventional ADI data reduction, and have not taken into account the effects of circumplanetary material on the detectability of embedded planets; Maire et al. 2017).

Other searches using ADI, carried out for planets forming in individual protoplanetary disks, have probed smaller orbital separations  $\sim 0.1''$  and lower companion luminosities (e.g., Quanz et al. 2013; Cieza et al. 2013; Currie et al. 2015; Testi et al. 2015; Canovas et al. 2017; Currie et al. 2017; Follette et al. 2017; Maire et al. 2017; Guidi et al. 2018; Keppler et al. 2018; Ligi et al. 2018; Reggiani et al. 2018; Sissa et al. 2018; Cugno et al. 2019; Gratton et al. 2019). Similarly, aperture masking has been used to probe even smaller separations (e.g., Biller et al. 2012; Kraus & Ireland 2012; Grady et al. 2013; Kraus et al. 2013; Sallum et al. 2015; Willson et al. 2016). The results of these observations are summarized in Table 1.

In addition to NIR searches for forming planets in disks, there have been several efforts to image  $H\alpha$  emission arising from the accretion shock on the forming planet. Several studies have targeted individual objects (HD 142527 – Close et al. 2014; LkCa 15 – Sallum et al. 2015; PDS70 – Haffert et al. 2019; Wagner et al. 2018). In a recent study, Zurlo et al. (2020) studied 11 nearby transition disks with SPHERE on the VLT and found no  $H\alpha$  emission from accreting planets down to an upper limit on accretion luminosity of  $10^{-6} L_\odot$  at  $0''.2$ , which

is about three orders of magnitude below the accretion luminosity inferred for LkCa 15b (Sallum et al. 2015).

Table 1 lists the 40 sources from the SEEDS study and the studies of individual disks that have been observed with angular differential imaging or aperture masking. Of these 24 are LMS and 16 are IMS (Column 2). Of the 40 sources, 20 have been classified as transition disks (Column 4). The 4 sources with two-arm spirals—the other signature of high-mass giant planets—are all transition disk sources. Column 5 provides the cavity size of the transition disks. Columns 6 and 7 list the inner and outer extent of the region of the disk that has been imaged. Columns 8-10 present the NIR magnitude of the stars, columns 11-13 present the contrast limits achieved at  $0''.25$ , and columns 14-16 present the measured value or upper limit on  $\lambda L_\lambda$  of a companion in each band. Assuming the colors of an accreting disk source (see Section 3), these upper limits are sufficient to detect a companion as bright as  $0.1L_\odot$  and sometimes much fainter.

The above studies have tended to focus on disks with spiral arms, gaps, and cavities, which are potential signposts of planets (e.g. Dong et al. 2015b,c). Unlike direct imaging searches for planets around stars without a disk, searches for planets in disk-bearing systems are complicated by the effect of the protoplanetary disk material on the detectability of embedded planets (e.g., Maire et al. 2017). As shown in the Table, most such efforts have yielded non-detections. For example, Maire et al. (2017) and Canovas et al. (2017) reported the non-detection of planets in the SAO 206462 and 2MASS J1604 disks, respectively, and placed an upper limit of a few Jupiter masses on the mass of putative planets at  $r \gtrsim 100$  AU in the former and at  $r \gtrsim 30$  AU in the latter.

Among these 40 systems, the most secure detection of accreting protoplanets is in PDS 70 (Keppler et al. 2018; Haffert et al. 2019). PDS 70 has detected companions at  $20.6 \pm 1.2$  au and  $34.5 \pm 2.0$  au (Haffert et al. 2019). The companions have been imaged in the NIR (Keppler et al. 2018),  $H\alpha$  (Wagner et al. 2018; Haffert et al. 2019), and their associated circumplanetary disks may have been discovered in mm continuum emission (Isella et al. 2019). From their  $H\alpha$  measurement, Wagner et al. (2018) estimate a planetary accretion rate of  $10^{-11 \pm 1} M_\odot \text{ yr}^{-1}$ . PDS 70 is a weak lined T Tauri star whose  $H\alpha$  equivalent width is  $\sim 2\text{\AA}$  (Gregorio-Hetem & Hetem 2002). Adopting the stellar parameters presented in Long et al. (2018) and the prescription for converting line luminosity to accretion luminosity given in Fang et al. (2009), we arrive at a stellar accretion rate of  $8 \times 10^{-11} M_\odot \text{ yr}^{-1}$ . For such low rates of accretion, it is possible that most of the  $H\alpha$  emission arises from

chromospheric activity, so this accretion rate should be taken as an upper limit. Over 5 Myr, only  $0.4 M_J$  would be accreted by the star at this rate. If they are hot start planets, the masses of PDS 70b and PDS 70c are estimated to be  $4 - 17 M_J$  and  $4 - 12 M_J$  respectively (Haffert et al. 2019) and the accretion rate would have been substantially higher in the past. There are significant uncertainties in both the planetary and stellar accretion rates, yet the derived values are consistent with a reasonable fraction of the accreting material through the disk being captured by the planet.

Multiple orbiting planetary companions have been reported in association with LkCa 15 (Kraus & Ireland 2012; Sallum et al. 2015), its three planetary candidates detected at  $\sim 15-20$  au in the inner cavity of its disk using NIR sparse aperture masking (SAM) (Sallum et al. 2015). One of these sources has been imaged in  $H\alpha$ , from which the accretion rate onto the planet has been estimated. The infrared colors and  $H\alpha$  emission are consistent with a planet mass times accretion rate  $M_p \dot{M}_p \sim 3 - 10 \times 10^{-6} M_J^2 yr^{-1}$ . For a Jovian mass companion, this translates to an accretion rate of  $\sim 3 - 10 \times 10^{-9} M_\odot yr^{-1}$ , which is within a factor of a few of the stellar accretion rate measured for LkCa 15 ( $3.6 \times 10^{-9} M_\odot yr^{-1}$ ; Ingleby et al. 2013). A subsequent study found that the  $H\alpha$  luminosity of the companion appears to vary, indicating variable accretion (Mendigutía et al. 2018). While there is significant uncertainty about the accretion rate onto the planet, the derived values are largely consistent with the expectation that a non-negligible fraction of the mass accreting through the disk makes it across the planet’s orbit into the inner disk (Lubow & D’Angelo 2006). While the detection of orbital motion in data taken over 6 years supports the interpretation that the emission arises from massive planetary companions (Sallum et al. 2015, Sallum et al. in prep.), other studies of LkCa 15 that use direct imaging techniques rather than SAM find structures that are more consistent with emission from an inner disk (Currie et al. 2019; Thalmann et al. 2016). Further study is needed to understand the properties of the orbiting emission sources.

One or more circumplanetary disks may have been detected in the HD 100546 system (Quanz et al. 2013; Brittain et al. 2013, 2014, 2015, 2019; Currie et al. 2015, 2017; Liskowsky et al. 2012). This system hosts a source of  $5\mu\text{m}$  CO fundamental emission located  $\sim 12$  au from the star, close to the inner rim of the outer disk, whose orbit has been followed for 15 yrs. The CO flux is consistent with emission from a circumplanetary disk with a radius of  $\sim 0.3$  AU if we assume the emitting gas is optically thick and at the same temperature as

the circumstellar gas near the disk edge (1400 K; Brittain et al. 2013). The temperature and emitting area are consistent with the theoretically predicted thermal properties of circumplanetary disks surrounding giant planets. Szulágyi et al. (2014) reported a disk temperature of  $\sim 2000$  K out to a Hill radius  $R_{\text{Hill}} \sim 0.8$  au for their case of a  $10 M_J$  planet at 5 au (see also Szulágyi 2017; Szulágyi & Mordasini 2017). Similar temperatures have been reported for the inner circumplanetary disk in other three-dimensional radiation hydrodynamical simulations (Klahr & Kley 2006; Gressel et al. 2013).

Confirmation of this source by direct imaging remains ambiguous. Currie et al. (2015) report the possible presence of a point source at the expected location of the CO emission, although the point source was not confirmed in subsequent observations (Follette et al. 2017; Rameau et al. 2017). One reason for the differing results may be because the point source fell behind the coronagraphic mask in the later observations (Currie et al. 2017). Attempts to detect the source with ALMA continuum imaging have also failed (Pineda et al. 2019), although it is likely that the pressure bump at the inner edge of the outer disk strongly filters out millimeter-sized dust grains and prevents them from reaching the circumplanetary disk. Moreover, grains that make it to the circumplanetary disk are expected to drift inward quickly (Zhu et al. 2018), enhancing the gas-to-dust ratio of the circumplanetary disk and leading to weak millimeter continuum emission. Thus the status of this possible planet remains uncertain. In addition to the source at  $\sim 12$  au, an extended source of IR emission has been reported at  $\sim 50$  au (Quanz et al. 2015), and a third millimeter continuum point source has been detected at 5.6 au with ALMA (Pérez et al. 2019).<sup>1</sup>

In summary, among the 20 sources studied to date that show signposts of giant planets (large cavities or two-arm spirals), accreting gas giant planets have been detected in at least 1 young LMS system (PDS 70) and possibly 1 additional young LMS system (LkCa 15) and 1 young IMS system (HD 100546; Table 2). These results correspond to a detection rate of 5–15% among this select group, whereas we would have expected to detect one or more giant planet companions in every system if all transition disks host multiple high-mass giant planets that radiate away their accretion energy as they form. In

<sup>1</sup> A companion candidate has very recently been detected in LBT  $L'$  and  $M$ -band imaging of the MWC 758 disk (Wagner et al. 2019). Assuming the emission is entirely photospheric, the planet is estimated to be 2–5  $M_J$  in mass in a hot-start scenario. No accretion signature has been detected from the candidate so far. As confirmation of the candidate is currently underway (K. Wagner, priv. comm.), we do not include this candidate in our study.

addition, no planetary companions have been reported in association with the remaining 20 non-transition disk sources in Table 1.

These results indicate that the incidence rate of bright, detectable giant planet companions among all stars is very low. That is, among young LMS, only 5-15% of their protoplanetary disks have transition disk SEDs (e.g., Muzerolle et al. 2010b; Furlan et al. 2011), and of the 12 young LMS transition disks in Table 1, only 1, possibly 2, have a bright detected companion, for a detection rate of 8-16%. The product of these two rates implies an incidence rate of accreting giant planetary companions to young LMS of  $\sim 1\%$ . Similarly, among IMS protoplanetary disks,  $\sim 40\%$  have transition disk SEDs (see Brittain et al. 2019, in preparation) and  $\sim 20\%$  have two-arm spirals (Dong et al. 2018a), whereas none or possibly one (HD 100546) of the 8 young IMS transition disks in Table 1 have a bright detected companion, for a detection rate of 0-12%. The product of these two rates implies an incidence rate of accreting giant planets of 0-5% for young IMS. In other words, the incidence rate of currently detectable accreting giant planet companions among all protoplanetary disks is likely of the order of a few percent.

### 3. TOY MODEL OF EPISODIC ACCRETION

It is perhaps surprising that the planet detection rate at these very young ages is so low, especially if most forming planets radiate away their accretion energy as they form (i.e., they are cold-start planets) and are expected to be bright in their mass-building phase. Here we explore the role episodic accretion may play in accounting for the dearth of bright young systems observed among these disks.

Lubow & Martin (2012) have noted that circumplanetary disks, like the more extended circumstellar disks in which they reside, are likely to harbor significant dead zones, i.e., regions that are insufficiently ionized to participate in accretion via the magnetorotational instability (MRI). As a result, as it is fed material from the circumstellar disk, the circumplanetary disk will grow in mass until it becomes gravitationally unstable. By driving turbulent heating (and thus ionization), gravitational instability warms the disk until it is sufficiently ionized thermally to drive accretion via the MRI, a process they refer to as the gravo-magneto instability (Armitage et al. 2001; Zhu et al. 2009; Martin & Lubow 2011). Their model predicts outburst rates ranging from  $0.04M_J \text{ yr}^{-1} - 2M_J \text{ yr}^{-1}$ , and quiescent rates ranging from  $4 \times 10^{-7}M_J \text{ yr}^{-1} - 3 \times 10^{-5}M_J \text{ yr}^{-1}$ , with accretion outbursts that last for several years occurring every  $10^4 - 10^5 \text{ yrs}$  (Lubow & D’Angelo 2006).

To compare the observed properties of detected accreting giant planets with the predictions of episodically accreting circumplanetary disks, we extend the work of Lubow & Martin (2012) by considering the effect of non-steady state disk accretion and the growing mass of the planet. To set the rate at which the circumplanetary disk is fed, we first consider a circumstellar disk with an accretion rate that declines with time as  $t^{-3/2}$ , mimicking the decline in the average measured stellar accretion rate over Myr timescales<sup>2</sup> (see for example Sicilia-Aguilar et al. 2005), such that

$$\dot{M}(t) = \dot{M}(t_0)(t/t_0)^{-3/2}. \quad (1)$$

We adopt  $t_0 = 1 \text{ Myr}$  and an initial accretion rate of  $\dot{M}(t_0) = 10^{-8} M_\odot \text{ yr}^{-1}$ , an accretion rate typical of young T Tauri stars (e.g., Hartmann et al. 1998). We then embed in the circumstellar accretion disk a forming giant planet with a mass  $M_p = 20M_\oplus$ , roughly the mass at which runaway accretion begins (e.g., D’Angelo et al. 2010).

From a theoretical perspective, the fraction of the accreting circumstellar disk material that is captured by the planet,  $f(M_p)$ , depends on a variety of parameters including  $q$ , the mass ratio of the planet and star, the orbital eccentricity of the companion, and the viscosity of the gas. Estimates from 2-dimensional simulations indicate that a forming gas giant planet captures 75%-90% of the accreting material (Lubow & D’Angelo 2006). However, the value is uncertain because the flow onto the planet and circumplanetary disk is intrinsically 3-dimensional (Ayliffe & Bate 2012; Batygin 2018; Tanigawa et al. 2012; Fung et al. 2015; Szulágyi et al. 2016).

Observationally, there are few constraints on the captured fraction, although we might attempt to infer its typical value from the ratio of the stellar and planetary accretion rates for the few accreting companions detected to date. As described in §2, the properties of the accreting companions to LkCa 15 and PDS 70 indicate that a significant portion of the material accreting through the disk is captured by the companion ( $\sim 50\%$  and  $\sim 10\%$  respectively), while only a small fraction of the mass is captured in the case of the companion to HD 142527 ( $\sim 10^{-3}$ ). These values are uncertain because the scaling relationship between H $\alpha$  emission and plan-

<sup>2</sup> As noted by Hartmann et al. (2016), although measured stellar accretion rates follow this declining trend, at stellar ages beyond  $\sim 3 \text{ Myr}$  most young stars have undetectable accretion. Our assumed rate of decline therefore overestimates the stellar accretion rate at late times, although this flaw has little impact on our results qualitatively. The effect of a steeper decline in the accretion rate is to fill the circumplanetary disk more slowly at later times resulting in more time between outbursts.

etary accretion rate may be in error, the accretion onto the planet may not be in steady state (e.g., Mendigutía et al. 2018), and/or the H $\alpha$  line may be more heavily extinguished by circumplanetary matter than estimated.

Given the uncertainties surrounding the captured fraction, we parameterize it as

$$f(M_p) = \frac{1}{1 + a/q}, \quad (2)$$

where  $a$  is a free parameter, and  $q = M_p/M_\star$  is the ratio of the companion mass to the mass of the central star. We arrived at this functional form and the value  $a = 10^{-4.5}$ , by fitting the relationship between  $f$  and  $q$  found in the 2-d hydrodynamical simulations presented by Lubow & D’Angelo (2006). Here we explore how the efficiency factor affects the duty cycle of accretion outbursts.

As material is captured by the forming planet, it fills a circumplanetary disk, which accretes onto the planet at a rate that depends on  $\zeta$ , the mass ratio of the circumplanetary disk to the forming planet. Here we assume

$$\begin{aligned} \dot{M}_p &= 5 \times 10^{-4} M_J \text{ yr}^{-1}; \text{ for } \zeta \gtrsim 0.1 \\ &= 5 \times 10^{-8} M_J \text{ yr}^{-1}; \text{ for } \zeta \lesssim 0.1. \end{aligned} \quad (3)$$

Although these rates are highly uncertain as well, they are based on measured accretion rates for young stars. While Lubow & Martin (2012) adopt much higher accretion rates in their outburst, Hall et al. (2019) find that in their models that for marginally gravitationally unstable disks, the accretion rate is of order  $10^{-7} M_\odot \text{ yr}^{-1}$  which we adopt for our model.

In quiescence, we assume that the accretion rate onto the planet is reduced by four orders of magnitude, consistent with the models of Lubow & Martin (2012). We allow the model to run until  $q = 5 \times 10^{-3}$ , at which point the forming companion halts accretion into its circumplanetary disk (Lubow et al. 1999; Lubow & D’Angelo 2006).

With these assumptions, the planet grows to  $9 M_J$  in about 3 Myr (Fig. 1b). The accretion luminosity of the planet alternates between  $\sim 4 \times 10^{-5} L_\odot$  and  $\sim 0.4 L_\odot$ . Outbursts occur every 1500 yr and last  $\sim 30$  yr; thus the circumplanetary disk spends  $\sim 2\%$  of the runaway accretion phase undergoing an outburst (Fig. 1a). Even in quiescence, the accretion luminosity exceeds the luminosity of a cold start planet ( $\sim 10^{-6} L_\odot$ ; Fortney et al. 2008). We can compare the accretion luminosity to the integrated luminosity of the detected companions orbiting HD 142527, LkCa 15, and PDS 70. We fit the disk accretion models by Zhu (2015) to the measured photometry for each source (Figure 2) and find that

their luminosities range from  $10^{-4} L_\odot$  to  $0.6 L_\odot$  (see Table 3 for the properties of the companions). The gray bars in figure 2 show the range of upper limits on  $\lambda L_\lambda$  of the sample in Table 1. Adopting the colors from the Zhu (2015) model, we find that the published observations are sufficiently sensitive to detect accreting circumplanetary disks with an integrated luminosity of  $10^{-4} - 0.1 L_\odot$ .

Thus, studies to date have imaged 20 disks with transition disk SEDs (4 of which have two-arm spirals) with sufficient sensitivity to detect a companion as bright as  $0.1 L_\odot$  (see §2). If each of the 20 disks harbors one accreting gas giant planet, and their circumplanetary disks are in outburst 2% of the time, we have a 33% chance of catching one or more circumplanetary disks in outburst. Dodson-Robinson & Salyk (2011) argued that the large cavity sizes of transition disks required the presence of multiple multi-Jupiter mass planets within the optically thin region. If each transition disk harbors two (three) accreting planets (and the observations probe the orbital radii of both/all planets), we have an 55% (70%) chance of catching one or more planets in outburst.

Interestingly, one companion as bright as our outburst luminosity ( $\sim 0.6 L_\odot$ ) has been detected to date, HD 142527B. In §4 we explore the possibility that HD 142527B is a planet surrounded by a circumplanetary disk in outburst. More generally though, the toy model suggests that episodic accretion can plausibly explain the low detection rate of accreting planetary companions to young stars. Future observational constraints on the incidence rate of giant planets and their luminosity in the accretion phase can directly constrain the duty cycle of episodic accretion and the outburst accretion rate.

In the episodic accretion picture, forming planets would present two faces to the world. Most of the time, they are accreting very slowly, they will look like a faint “cold start” planet surrounded by a quiescent disk. A small fraction of the time (a few %), when in outburst, the emission from system will be dominated by emission from the disk, as in an FU Ori object, with the color and luminosity of an M star. In the next section, we discuss whether the directly imaged companion to HD 142527 could be in the latter state.

#### 4. HD 142527: STELLAR OR PLANETARY COMPANION?

The directly imaged companion to the young F6 star HD 142527 ( $2.0 \pm 0.3 M_\odot$ ) has been detected through its NIR continuum and H $\alpha$  emission at a separation of  $\sim 13$  au from the star (Biller et al. 2012; Close et al. 2014). A spectrum of the companion in the  $H$ - and  $K$ -

bands has also been acquired (Christiaens et al. 2018). These observations have been interpreted as emission from a young M2.5 star with a mass of  $\sim 0.1\text{--}0.4 M_{\odot}$  that is accreting at a rate  $6 \times 10^{-10} M_{\odot} \text{ yr}^{-1}$  (Close et al. 2014; Lacour et al. 2016; Biller et al. 2012; Christiaens et al. 2018), a tiny fraction of the accretion rate onto this  $5.0 \pm 1.5$  Myr old star ( $\sim 2 \times 10^{-7} M_{\odot} \text{ yr}^{-1}$ ) (Mendigutía et al. 2014).

Studies that have used dynamical arguments to constrain the mass of the companion favor a stellar companion, although the constraints admit the possibility of one or more planetary mass companions instead (Price et al. 2018; Claudi et al. 2019; see §5 for further details). In the absence of strong evidence to the contrary, we here consider the possibility that the companion is a planetary mass companion surrounded by a circumplanetary disk undergoing an accretion outburst. Earlier studies have suggested that the NIR spectrum of an active accretion disk can mimic that of an M-star (e.g., Herbig 1977; see also Zhu 2015).

Figure 2a compares the IR photometry of the companion (black points; Lacour et al. 2016) with the model spectrum of an accreting circumplanetary disk (black spectrum). In the model, the circumplanetary disk accretes at a constant rate onto the planet. The effective temperature of the circumplanetary disk is the standard steady optically thick accretion disk temperature. The vertical temperature dependence of the disk atmosphere at each radius is calculated using the gray-atmosphere approximation in the Eddington limit, adopting the Rosseland mean optical depth. With the temperature determined at each radius, the SED of the local annulus is calculated. By summing the SEDs from different annuli, the SED of the accretion disk is obtained (Zhu 2015).

The other model parameters—in addition to the disk accretion rate and the range of disk radii that contribute to the emission—are the disk inclination and the reddening to the disk. The inclination of the outer disk around HD 142527 is  $\sim 20\text{--}30^{\circ}$  (Pontoppidan et al. 2011; Casassus et al. 2013), whereas the inner circumstellar disk is inferred to have an inclination  $\sim 70^{\circ}$  relative to the outer disk (Marino et al. 2015). If the companion has a disk, it is not clear what the orientation of the disk would be, so its inclination is treated as a free parameter in our fit. The planet and circumplanetary disk are expected to be embedded in a circumplanetary envelope (Tanigawa et al. 2012; Gressel et al. 2013; Szulágyi et al. 2016) that may extinct and redden the emission from the planet+disk by an unknown amount. We therefore assume a parameterized reddening

law  $A_{\lambda} = A_J(\lambda/1.235)^{-\alpha}$  where  $A_J$  and  $\alpha$  are free parameters.

In the model calculation, the inclination correction is treated simply as a multiplicative factor that corrects for the projected disk emitting area. We obtain a reasonable fit with a disk that extends from an inner radius of  $R_{in} = 1.5R_J$  to an outer radius of  $R_{out} = 15R_J$ , an accretion rate  $\dot{M}_p$  such that  $M_p \dot{M}_p = 10^{-2} M_J^2 \text{ yr}^{-1}$ , where  $M_p$  is the planetary mass, and extinction and inclination parameters of  $A_J = 1.6$ ,  $\alpha = 1.7$ , and  $i = 70^{\circ}$  (Fig. 2a).

To compare the model to the NIR spectrum of the companion (Christiaens et al. 2018), we assume the absolute flux calibration of the photometry is more reliable than the spectrum, so we scale the spectrum to be consistent with the photometry. The model and scaled spectrum agree well (Figure 2), although there is a slight discrepancy in the  $K$ -band region. Such differences are not surprising, because of the simple assumptions made in the model. For example, the model assumes a simple vertical temperature structure (based on a grey atmosphere with no temperature correction; Zhu 2015). Any deviation from the standard radial disk temperature profile assumed here will also alter the SED. Furthermore, the opacity of the model is fixed at solar abundance and an adopted mean opacity, so any changes in the elemental composition of the accreting material would affect the SED. For example, any trapping of large grains in pressure bumps in the circumstellar disk will reduce the dust content of the material accreting into circumplanetary disk.

These results show that the emission properties of the companion to HD 142527 are plausibly those of a giant planet surrounded by a circumplanetary disk that is undergoing an accretion outburst and whose emission dominates the emission from the planet. If the companion is in fact a  $10 M_J$  planet surrounded by a circumplanetary disk, then our fit value of  $M_p \dot{M}_p = 10^{-2} M_J^2 \text{ yr}^{-1}$  implies a planetary accretion rate of  $10^{-6} M_{\odot} \text{ yr}^{-1}$ , roughly an order of magnitude higher than the stellar accretion rate for this system (Mendigutía et al. 2014).

## 5. DISCUSSION

In §1, we argued that the high incidence rate of disk substructure indicating the presence of massive ( $\sim 5M_J$ ) giant planets (e.g., two-arm spirals and transition disk morphologies associated with  $\sim 10\text{--}20\%$  of disk-bearing stars) coupled with the lack of directly imaged “hot start” planets in this mass range at  $> 10$  Myr ages, suggests that giant planets form “cold start”, i.e., that planets radiate away much their accretion energy in the accretion phase. The lack of evidence for energy loss in this form, i.e., the ready detection of bright, accreting

planets in the pre-main-sequence phase ( $\sim 1$  Myr), led us to propose that planets accrete their mass episodically, through punctuated outbursts of accretion in the runaway gas accretion phase.

This interpretation may appear too glib when we consider that some of the first directly imaged planets, those orbiting  $\beta$  Pic and HR 8799, appear to be “hot start” planets. Dynamical constraints on their masses, coupled with their observed luminosities, are consistent with the predictions of hot start models (Fabrycky & Murray-Clay 2010; Wang et al. 2018). While these planets were first reported many years ago (Marois et al. 2008; Lagrange et al. 2009), subsequent discoveries of directly imaged planets have been few and far between (Bowler 2016; Stone et al. 2018; Nielsen et al. 2019).

One interpretation of the discrepancy between these results is that planet formation proceeds through multiple pathways. Planet formation via gravitational instability, which favors high mass planets ( $> 10M_J$ ), is expected to produce hot start planets, while core accretion, which favors low mass planets ( $< 10M_J$ ), is expected to produce colder start planets. Both pathways may lead to 5–15  $M_J$  planets at the orbital separations probed by direct imaging, with the brighter hot start planets readily detected ( $\beta$  Pic, HR 8799) and the (possibly more numerous) cold start planets as yet unprobed.

The episodic accretion scenario described in §3 predicts that accreting planets will come in two flavors: (1) outbursting systems with such high disk accretion rates that their emission is dominated by the circumplanetary disk and has the color of low mass stars and (2) systems that are faint because the circumplanetary disk is inactive. At a planet mass of  $\sim 3M_J$ —the mass of the multiple planets invoked by Dodson-Robinson & Salyk (2011) to explain the large cavities of transition disks—the outbursting state in our toy model corresponds to  $M_p\dot{M}_p=1.5 \times 10^{-3} M_J^2 \text{ yr}^{-1}$  and is sufficiently bright to have been detected by the 40 published observations of disks (Figure 2b, Table 1). The quiescent state for such a  $3M_J$  planet corresponds to  $M_p\dot{M}_p=1.5 \times 10^{-7} M_J^2 \text{ yr}^{-1}$  or about two orders of magnitude fainter at  $K$ -band than the most sensitive published observations to date (Fig. 2). As with young stars, there is likely a large range of accretion rates that represent the quiescent, steady-state rate of circumplanetary disks. Because quiescent disks are faint in the NIR and emit more of their energy in the MIR, searches at longer wavelengths may be better able to detect quiescent disks (Fig. 2; see also Szulágyi et al. 2019).

While the emission properties of HD 142527b are plausibly consistent with those of a circumplanetary disk in outburst (Fig. 2b), the companions PDS 70bc and

LkCa 15bc have fluxes between the outburst and quiescent states of our model. We hypothesize that these values reflect the upper limit of the range of quiescent states rather than the lower range for outbursting disks, because it is unlikely that two circumplanetary disks in a given system would undergo an outburst simultaneously.

Other authors have described how the HD 142527 system properties are consistent with a stellar, rather than planetary, companion (e.g., Biller et al. 2012; Lacour et al. 2016; Christiaens et al. 2018). A stellar companion is consistent with many detailed aspects of the system: the multiple spiral arms in the outer disk at  $r \gtrsim 100$  au (Fukagawa et al. 2006; Canovas et al. 2013), the large central clearing in the disk ( $\sim 1''$  radius; Fukagawa et al. 2013), the azimuthal asymmetry in the outer disk (Casassus et al. 2013), and evidence for a (spatially unresolved) inner disk that is highly misaligned with the outer disk (Marino et al. 2015). Price et al. (2018) proposed that these properties can be explained by a single companion that has a mass of  $0.4 M_\odot$  and an unusual orbit, with both high eccentricity ( $e=0.6$ – $0.7$ ) and an inclination that is almost polar with respect to the outer disk.

Price et al. (2018) state that their results are not strongly sensitive to the companion mass in the range they studied, and a lower, planetary mass companion (e.g.,  $\sim 10M_J$ ) is not clearly excluded. Lacour et al. (2016) and Claudi et al. (2019) have shown that both the mass and the orbit of the companion are highly uncertain. For example, Claudi et al. (2019) placed a dynamical constraint on the mass of the companion of  $0.26_{-0.14}^{+0.16} M_\odot$ . Thus the analysis favors a stellar companion but does not rule out a  $10M_J$  companion. It is also unclear whether all of the circumstellar disk properties are the result of a single companion. A disk with a very large inner hole, like that of HD 142527, could signal the presence of multiple giant planet companions (Zhu et al. 2011; Dodson-Robinson & Salyk 2011); perhaps the best example of this is PDS 70bc (Haffert et al. 2019). Thus available data allow for the possibility of a planetary mass companion.

The episodic accretion picture can be tested by searching for orbiting companions in their more typical, quiescent state, with deeper high contrast imaging than has been performed to date. Orbiting companions may also be identified through submillimeter continuum imaging of circumplanetary disks, infrared imaging and spectroscopy of circumplanetary disks, and Gaia astrometry.

ALMA may be able to detect quiescently accreting circumplanetary disks through their dust emission (e.g., Zhu et al. 2018; Boehler et al. 2017; Isella et al. 2014),

however the strength of the emission depends on the extent to which disk solids are filtered out by gap edge of the outer disk (e.g., Rice et al. 2006) before reaching the circumplanetary disk. Efficient filtering or rapid growth into large solids will reduce the circumplanetary disk optical depth, potentially compromising the detectability of the dust emission signature. Perhaps as a result, circumplanetary disk detections with this approach have been rare to date despite multiple attempts. An exciting possible detection has been reported by Pérez et al. (2019) in the HD 100546 system.

Circumplanetary disks can also be detected and studied in the infrared. Quiescent circumplanetary disks can potentially be detected through gas emission features from their atmosphere, e.g., with spectroastrometry of  $5\ \mu\text{m}$  CO fundamental emission as in HD 100546 (Brittain et al. 2019). Future observations can potentially also distinguish between the stellar vs. outbursting circumplanetary disk explanations for the detected companion to HD 142527, e.g., by using infrared spectroscopy to measure the gravity of the companion. Compared to the dwarf-like gravity expected for a young low-mass companion, accretion disks in outburst are expected to show giant-like gravity, e.g., in their  $2.3\ \mu\text{m}$  CO overtone absorption (e.g., FU Ori; Kenyon & Hartmann 1995). More sensitive searches for companions to much larger samples of young stars will be possible with imagers on 30-m class telescopes. Zhu (2015) and Szulágyi et al. (2019) suggest that the mid-infrared observations will be more sensitive to the presence of forming planets and their circumplanetary disks than the near-infrared observations pursued thus far. Mid-infrared observations are not only better matched to the spectral region where much of the flux is emitted, they are also less sensitive to potential obscuration by dust in the surrounding protoplanetary disk environment.

One might wonder whether significant obscuration can explain the low detection rate of forming planets, obviating the need for episodic accretion. At first glance, it seems unlikely that extinction by the circumstellar disk can account for the observational results. Simulations of gap opening show that even relatively low-mass planets ( $\sim 0.5\ M_{\text{J}}$ ) in a modest viscosity environment ( $\alpha = 10^{-3}$ ) are able to clear a gap to  $\sim 3\%$  of its original density (Fung et al. 2014). For a gap in a transition disk reduced in column density by a roughly a factor of 100-10,000 relative to the MMSN (van der Marel et al. 2016; Furlan et al. 2011), this results in negligible near-infrared (i.e., K-band) extinction of the forming planet ( $\lesssim 0.05$  mag). Once the planet grows to greater than a Jupiter mass, this problem becomes even less severe, so it is plausible that circumstellar disk extinction does

not account for the dearth of forming planets imaged in disks. Longer wavelength observations can test this picture.

One particularly promising way to identify weakly or non-accreting gas giant planets in disks is through the use of *Gaia* astrometry. This method has already been used to measure the mass of the gas giant orbiting the A-star  $\beta$  Pic. The current data from *Gaia* and *Hipparcos* are able to detect the stellar reflex motion induced by an orbiting 11–13  $M_{\text{J}}$  planet in an A star 20 pc away with a precision of 3  $M_{\text{J}}$  (Snellen & Brown 2018; Dupuy et al. 2019). A similar approach can be used to measure the mass of the companion to HD 142527 and test our scenario that it is an accreting planet rather than a star. Once the full *Gaia* time baseline becomes available, along with the expected 100-fold increase in astrometric precision, it should be possible to detect the stellar reflex motion of a sub-Jovian mass planet ( $\geq 0.3\ M_{\text{J}}$ ) at the distance of HD 142527 (157 pc) or definitively rule out a substellar mass for the companion.

Finally, an observational campaign focused on a larger sample of sources, especially those with dynamical signatures of massive planets (large and deep cavities or two-arm spirals), will constrain the duty cycle and magnitude of outbursts. The fraction of bright circumplanetary disks detected in outburst reflects the duty cycle of the outbursts, which depends on the rate at which the circumplanetary disk grows and the rate at which it empties. As the rate of accretion onto the circumplanetary disk increases, so does the frequency of outbursts, if their magnitude and duration remain the same. If outbursts are more violent than we assume (with planetary accretion rates of  $\dot{M}_p \gtrsim 10^{-6}\ M_{\odot}\ \text{yr}^{-1}$ ), they will be brighter and the duty cycle lower. Surveys that report upper limits on the luminosity of companions in systems that are expected to harbor gas giant planets are crucial for advancing our understanding of this very important phase of gas giant planet growth.

We are grateful to Scott Kenyon for comments on an early version of this manuscript. This work was performed in part at the Aspen Center for Physics which is supported by the National Science Foundation grant PHY-1607611. Work by SDB was performed in part at the National Optical Astronomy Observatory. NOAO is operated by the Association of Universities for Research in Astronomy (AURA), Inc. under a cooperative agreement with the National Science Foundation. SDB also acknowledges support from this work by NASA Agreement No. NXX15AD94G; NASA Agreement No. NNX16AJ81G; and NSF-AST 1517014.

## REFERENCES

- Akiyama, E., Hashimoto, J., Liu, H. B., et al. 2016, *AJ*, 152, 222
- ALMA Partnership, Brogan, C. L., Pérez, L. M., et al. 2015, *ApJL*, 808, L3
- Armitage, P. J., Livio, M., & Pringle, J. E. 2001, *MNRAS*, 324, 705
- Avenhaus, H., Quanz, S. P., Garufi, A., et al. 2018, *ApJ*, 863, 44
- Ayliffe, B. A., & Bate, M. R. 2012, *MNRAS*, 427, 2597
- Baraffe, I., Chabrier, G., Barman, T. S., Allard, F., & Hauschildt, P. H. 2003, *A&A*, 402, 701
- Batygin, K. 2018, *AJ*, 155, 178
- Biller, B., Lacour, S., Juhász, A., et al. 2012, *ApJL*, 753, L38
- Boehler, Y., Weaver, E., Isella, A., et al. 2017, *ApJ*, 840, 60
- Bowler, B. P. 2016, *PASP*, 128, 102001
- Brittain, S. D., Carr, J. S., Najita, J. R., Quanz, S. P., & Meyer, M. R. 2014, *ApJ*, 791, 136
- Brittain, S. D., & Najita, J. R. 2019, *ApJ*, submitted
- Brittain, S. D., Najita, J. R., & Carr, J. S. 2015, *Ap&SS*, 357, 54
- . 2019, *ApJ*, 883, 37
- Brittain, S. D., Najita, J. R., Carr, J. S., et al. 2013, *ApJ*, 767, 159
- Canovas, H., Ménard, F., Hales, A., et al. 2013, *A&A*, 556, A123
- Canovas, H., Hardy, A., Zurlo, A., et al. 2017, *A&A*, 598, A43
- Canovas, H., Montesinos, B., Schreiber, M. R., et al. 2018, *A&A*, 610, A13
- Casassus, S., Hales, A., de Gregorio, I., et al. 2013, *A&A*, 553, A64
- Cassan, A., Kubas, D., Beaulieu, J.-P., et al. 2012, *Nature*, 481, 167
- Christiaens, V., Casassus, S., Absil, O., et al. 2018, *A&A*, 617, A37
- Cieza, L. A., Lacour, S., Schreiber, M. R., et al. 2013, *ApJ*, 762, L12
- Clarke, C. J., Tazzari, M., Juhasz, A., et al. 2018, *ApJL*, 866, L6
- Claudi, R., Maire, A. L., Mesa, D., et al. 2019, *A&A*, 622, A96
- Close, L. M., Follette, K. B., Males, J. R., et al. 2014, *ApJL*, 781, L30
- Cugno, G., Quanz, S. P., Hunziker, S., et al. 2019, *A&A*, 622, A156
- Cumming, A., Butler, R. P., Marcy, G. W., et al. 2008, *PASP*, 120, 531
- Currie, T., Brittain, S., Grady, C. A., Kenyon, S. J., & Muto, T. 2017, *Research Notes of the American Astronomical Society*, 1, 40
- Currie, T., Cloutier, R., Brittain, S., et al. 2015, *ApJL*, 814, L27
- Currie, T., & Sicilia-Aguilar, A. 2011, *ApJ*, 732, 24
- Currie, T., Marois, C., Cieza, L., et al. 2019, *ApJL*, 877, L3
- D'Angelo, G., Durisen, R. H., & Lissauer, J. J. 2010, *Giant Planet Formation*, ed. S. Seager, 319–346
- Dodson-Robinson, S. E., & Salyk, C. 2011, *ApJ*, 738, 131
- Dong, R., & Fung, J. 2017, *ApJ*, 835, 38
- Dong, R., Hall, C., Rice, K., & Chiang, E. 2015a, *ApJL*, 812, L32
- Dong, R., Najita, J. R., & Brittain, S. 2018a, *ApJ*, 862, 103
- Dong, R., Zhu, Z., Rafikov, R. R., & Stone, J. M. 2015b, *ApJL*, 809, L5
- Dong, R., Zhu, Z., & Whitney, B. 2015c, *ApJ*, 809, 93
- Dong, R., Liu, S.-y., Eisner, J., et al. 2018b, *ApJ*, 860, 124
- Dupuy, T. J., Brandt, T. D., Kratter, K. M., & Bowler, B. P. 2019, *ApJL*, 871, L4
- Eisner, J. A. 2015, *ApJL*, 803, L4
- Espaillet, C., Muzerolle, J., Najita, J., et al. 2014a, *Protostars and Planets VI*, 497
- Espaillet, C., Muzerolle, J., Najita, J., et al. 2014b, in *Protostars and Planets VI*, ed. H. Beuther, R. S. Klessen, C. P. Dullemond, & T. Henning, 497
- Fabrycky, D. C., & Murray-Clay, R. A. 2010, *ApJ*, 710, 1408
- Fang, M., van Boekel, R., Wang, W., et al. 2009, *A&A*, 504, 461
- Follette, K. B., Rameau, J., Dong, R., et al. 2017, *AJ*, 153, 264
- Fortney, J. J., Marley, M. S., Saumon, D., & Lodders, K. 2008, *ApJ*, 683, 1104
- Fukagawa, M., Tamura, M., Itoh, Y., et al. 2006, *ApJL*, 636, L153
- Fukagawa, M., Tsukagoshi, T., Momose, M., et al. 2013, *PASJ*, 65, L14
- Fung, J., Artymowicz, P., & Wu, Y. 2015, *ApJ*, 811, 101
- Fung, J., & Dong, R. 2015, *ApJL*, 815, L21
- Fung, J., Shi, J.-M., & Chiang, E. 2014, *ApJ*, 782, 88
- Furlan, E., Luhman, K. L., Espaillet, C., et al. 2011, *ApJS*, 195, 3
- Grady, C. A., Polomski, E. F., Henning, T., et al. 2001, *AJ*, 122, 3396
- Grady, C. A., Muto, T., Hashimoto, J., et al. 2013, *ApJ*, 762, 48
- Gratton, R., Ligi, R., Sissa, E., et al. 2019, *A&A*, 623, A140
- Gregorio-Hetem, J., & Hetem, A. 2002, *MNRAS*, 336, 197

- Gressel, O., Nelson, R. P., Turner, N. J., & Ziegler, U. 2013, *ApJ*, 779, 59
- Guidi, G., Ruane, G., Williams, J. P., et al. 2018, *MNRAS*, 479, 1505
- Haffert, S. Y., Bohn, A. J., de Boer, J., et al. 2019, *Nature Astronomy*, 329
- Hall, C., Dong, R., Rice, K., et al. 2019, *ApJ*, 871, 228
- Hall, C., Rice, K., Dipierro, G., et al. 2018, *MNRAS*, 477, 1004
- Hartmann, L., Calvet, N., Gullbring, E., & D'Alessio, P. 1998, *ApJ*, 495, 385
- Hartmann, L., Herczeg, G., & Calvet, N. 2016, *ARA&A*, 54, 135
- Herbig, G. H. 1977, *ApJ*, 217, 693
- Ingleby, L., Calvet, N., Herczeg, G., et al. 2013, *ApJ*, 767, 112
- Isella, A., Benisty, M., Teague, R., et al. 2019, *ApJL*, 879, L25
- Isella, A., Chandler, C. J., Carpenter, J. M., Pérez, L. M., & Ricci, L. 2014, *ApJ*, 788, 129
- Jensen, E. L. N., Cohen, D. H., & Gagné, M. 2009, *ApJ*, 703, 252
- Johnson, J. A., Howard, A. W., Bowler, B. P., et al. 2010, *PASP*, 122, 701
- Kenyon, S. J., & Hartmann, L. 1995, *ApJS*, 101, 117
- Kenyon, S. J., Hartmann, L. W., Strom, K. M., & Strom, S. E. 1990, *AJ*, 99, 869
- Keppler, M., Benisty, M., Müller, A., et al. 2018, *A&A*, 617, A44
- Klahr, H., & Kley, W. 2006, *A&A*, 445, 747
- Kratter, K., & Lodato, G. 2016, *ARA&A*, 54, 271
- Kraus, A. L., & Ireland, M. J. 2012, *ApJ*, 745, 5
- Kraus, S., Ireland, M. J., Sitko, M. L., et al. 2013, *The Astrophysical Journal*, 768, 80
- Lacour, S., Biller, B., Cheetham, A., et al. 2016, *A&A*, 590, A90
- Lagrange, A.-M., Gratadour, D., Chauvin, G., et al. 2009, *A&A*, 493, L21
- Ligi, R., Vigan, A., Gratton, R., et al. 2018, *MNRAS*, 473, 1774
- Liskowsky, J. P., Brittain, S. D., Najita, J. R., et al. 2012, *ApJ*, 760, 153
- Long, Z. C., Akiyama, E., Sitko, M., et al. 2018, *ApJ*, 858, 112
- Lubow, S. H., & D'Angelo, G. 2006, *ApJ*, 641, 526
- Lubow, S. H., & Martin, R. G. 2012, *ApJL*, 749, L37
- Lubow, S. H., Seibert, M., & Artymowicz, P. 1999, *ApJ*, 526, 1001
- Luhn, J. K., Bastien, F. A., Wright, J. T., et al. 2018, *ArXiv e-prints*, arXiv:1811.03043
- Maire, A. L., Stolker, T., Messina, S., et al. 2017, *A&A*, 601, A134
- Malfait, K., Bogaert, E., & Waelkens, C. 1998, *A&A*, 331, 211
- Marino, S., Perez, S., & Casassus, S. 2015, *ApJL*, 798, L44
- Marley, M. S., Fortney, J. J., Hubickyj, O., Bodenheimer, P., & Lissauer, J. J. 2007, *ApJ*, 655, 541
- Marois, C., Macintosh, B., Barman, T., et al. 2008, *Science*, 322, 1348
- Martin, R. G., & Lubow, S. H. 2011, *ApJL*, 740, L6
- Mawet, D., Choquet, É., Absil, O., et al. 2017, *AJ*, 153, 44
- Mendigutía, I., Fairlamb, J., Montesinos, B., et al. 2014, *ApJ*, 790, 21
- Mendigutía, I., Oudmaijer, R. D., Schneider, P. C., et al. 2018, *A&A*, 618, L9
- Muto, T., Grady, C. A., Hashimoto, J., et al. 2012, *ApJL*, 748, L22
- Muzerolle, J., Allen, L. E., Megeath, S. T., Hernández, J., & Gutermuth, R. A. 2010a, *ApJ*, 708, 1107
- . 2010b, *ApJ*, 708, 1107
- Nielsen, E. L., De Rosa, R. J., Macintosh, B., et al. 2019, *AJ*, 158, 13
- Pérez, S., Casassus, S., Hales, A., et al. 2019, *arXiv e-prints*, arXiv:1906.06305
- Pineda, J. E., Szulágyi, J., Quanz, S. P., et al. 2019, *ApJ*, 871, 48
- Pontoppidan, K. M., Blake, G. A., & Smette, A. 2011, *ApJ*, 733, 84
- Price, D. J., Cuello, N., Pinte, C., et al. 2018, *MNRAS*, 477, 1270
- Quanz, S. P., Amara, A., Meyer, M. R., et al. 2015, *ApJ*, 807, 64
- . 2013, *ApJL*, 766, L1
- Rameau, J., Follette, K. B., Pueyo, L., et al. 2017, *AJ*, 153, 244
- Reggiani, M., Christiaens, V., Absil, O., et al. 2018, *A&A*, 611, A74
- Rice, W. K. M., Armitage, P. J., Wood, K., & Lodato, G. 2006, *MNRAS*, 373, 1619
- Sallum, S., Follette, K. B., Eisner, J. A., et al. 2015, *Nature*, 527, 342
- Sicilia-Aguilar, A., Hartmann, L. W., Hernández, J., Briceño, C., & Calvet, N. 2005, *AJ*, 130, 188
- Sissa, E., Gratton, R., Garufi, A., et al. 2018, *A&A*, 619, A160
- Snellen, I. A. G., & Brown, A. G. A. 2018, *Nature Astronomy*, 2, 883
- Stone, J. M., Skemer, A. J., Hinz, P. M., et al. 2018, *ArXiv e-prints*, arXiv:1810.10560
- Szulágyi, J. 2017, *ApJ*, 842, 103

- Szulágyi, J., Dullemond, C. P., Pohl, A., & Quanz, S. P. 2019, *MNRAS*, 487, 1248
- Szulágyi, J., Masset, F., Lega, E., et al. 2016, *MNRAS*, 460, 2853
- Szulágyi, J., Morbidelli, A., Crida, A., & Masset, F. 2014, *ApJ*, 782, 65
- Szulágyi, J., & Mordasini, C. 2017, *MNRAS*, 465, L64
- Tang, Y.-W., Guilloteau, S., Dutrey, A., et al. 2017, *ApJ*, 840, 32
- Tanigawa, T., Ohtsuki, K., & Machida, M. N. 2012, *ApJ*, 747, 47
- Testi, L., Skemer, A., Henning, T., et al. 2015, *ApJ*, 812, L38
- Thalmann, C., Janson, M., Garufi, A., et al. 2016, *ApJL*, 828, L17
- Uyama, T., Hashimoto, J., Kuzuhara, M., et al. 2017, *AJ*, 153, 106
- van der Marel, N., Verhaar, B. W., van Terwisga, S., et al. 2016, *A&A*, 592, A126
- Wagner, K., Stone, J. M., Spalding, E., et al. 2019, *ApJ*, 882, 20
- Wagner, K., Follete, K. B., Close, L. M., et al. 2018, *ApJL*, 863, L8
- Wang, J. J., Graham, J. R., Dawson, R., et al. 2018, *AJ*, 156, 192
- Willson, M., Kraus, S., Kluska, J., et al. 2016, *A&A*, 595, A9
- Zhang, K., Bergin, E. A., Blake, G. A., et al. 2016, *ApJL*, 818, L16
- Zhu, Z. 2015, *ApJ*, 799, 16
- Zhu, Z., Andrews, S. M., & Isella, A. 2018, *MNRAS*, 479, 1850
- Zhu, Z., Hartmann, L., & Gammie, C. 2009, *ApJ*, 694, 1045
- Zhu, Z., Ju, W., & Stone, J. M. 2016, *ApJ*, 832, 193
- Zhu, Z., Nelson, R. P., Hartmann, L., Espaillat, C., & Calvet, N. 2011, *ApJ*, 729, 47
- Zurlo, A., Cugno, G., Montesinos, M., et al. 2020, *A&A*, 633, A119

Star	Type	Distance	Morphology <sup>a</sup>		Cavity		Inner		Outer		Stellar					Contrast					$\lambda L_{\lambda}$		
			[1]	[2]	[3]	[4]	[5]	[6]	[7]	[8]	[9]	[10]	[11]	[12]	[13]	[14]	[15]	[16]	[17]	[18]	[19]	[20]	
		pc	Size	Extent	Extent	au	au	H	K <sub>S</sub>	L	$\Delta$	H	$\Delta K_S$	$\Delta L$	H	K <sub>S</sub>	L	$\Delta K_S$	$\Delta L$	H	K <sub>S</sub>	L	
AB Aur <sup>1</sup>	IMS	163 ± 9	T <sup>25</sup> , MSp <sup>26</sup>	70	32.6	489.0	5.082	4.23	3.254	—	—	—	2.09E-03	—	—	≤ 1.27E+32	—	—	—	—	—	—	
DM Tau <sup>1,2</sup>	LMS	145 ± 7	T <sup>25</sup>	19	5.8	435.0	9.757	9.522	9.458	1.00E-02	—	—	—	—	≤ 6.02E+30	—	—	—	—	—	—	—	
LMS Aur <sup>1</sup>	LMS	160 ± 13	T <sup>25</sup>	28	16.0	480.0	8.603	8.283	8.369	7.59E-04	—	—	—	—	≤ 1.60E+30	—	—	—	—	—	—	—	
LkHa 330 <sup>2</sup>	IMS	311 ± 24	T <sup>25</sup> , 2Sp <sup>27</sup>	68	62.2	62.2	7.917	7.03	6.072	—	—	—	5.75E-03	—	—	≤ 9.68E+31	—	—	—	—	—	—	
HD100546 <sup>3-7</sup>	IMS	110 ± 6	T <sup>28</sup> , MSp <sup>29</sup>	13	11.0	88.0	5.962	5.418	4.201	2.51E-04	—	—	—	—	≤ 2.86E+30	—	—	—	—	—	—	—	
MWC 758 <sup>3,8,9</sup>	IMS	160 ± 11	T <sup>25</sup> , 2Sp <sup>30</sup>	73	16.0	176.0	6.56	5.804	4.599	—	—	—	1.00E-04	—	≤ 1.38E+30	—	—	—	—	—	—	—	
SAO 206462 <sup>3,10</sup>	IMS	136 ± 10	T <sup>25</sup> , 2Sp <sup>31</sup>	46	13.6	272.0	6.587	5.843	5.046	2.00E-05	—	—	1.00E-04	—	≤ 9.57E+29	—	—	—	—	—	—	—	
HD169142 <sup>3,11,12</sup>	IMS	114 ± 7	T <sup>25</sup> , MSp <sup>32</sup>	20	11.4	114.0	6.41	5.995	1.32E-04	—	—	—	1.32E-04	—	≤ 5.28E+29	—	—	—	—	—	—	—	
TW Hya <sup>2,3</sup>	LMS	60.1 ± 2.5	T <sup>25</sup>	4	1.2	12.0	7.558	7.297	7.101	—	—	—	6.31E-03	—	≤ 3.10E+30	—	—	—	—	—	—	—	
HD 141569 <sup>13</sup>	IMS	111 ± 1	T <sup>33</sup>	20	11.1	276.6	—	—	—	—	—	—	—	—	≤ 30M <sub>J</sub> at L-band	—	—	—	—	—	—	—	
HD 142527 <sup>14</sup>	IMS	157 ± 1	T <sup>25</sup>	140	31.4	471.0	5.715	4.980	4.280	—	—	—	—	4.39E+32	—	—	—	—	—	—	—	8.12E+31	
PDS 70b <sup>15,16</sup>	LMS	113 ± 5	T <sup>25</sup>	60	17.0	113.0	8.823	8.542	8.026	—	—	—	6.31E-04	1.74E-03	2.35E+32	—	—	—	—	—	—	—	3.51E+29
PDS 70c <sup>16</sup>	LMS	159 ± 8	T <sup>25</sup>	50	8.0	31.8	8.823	8.542	8.026	—	—	—	3.02E-04	2.29E-03	1.68E+29	—	—	—	—	—	—	—	5.46E+29
LkCa 15b <sup>1,17,18</sup>	LMS	188 ± 10	T <sup>34</sup>	15	5.6	56.4	8.600	8.163	7.49	5.25E-03	—	—	3.98E-04	1.00E-02	6.16E+30	—	—	—	—	—	—	—	7.72E+30
FL Cha (T35) <sup>19</sup>	LMS	128 ± 7	T <sup>35</sup>	15	6.4	25.6	9.175	8.873	8.38	—	—	—	1.20E-02	—	≤ 1.09E+31	—	—	—	—	—	—	—	—
FP Tau <sup>2</sup>	LMS	100.83 ± 0.26	T, 2Sp <sup>27</sup>	7	4.0	80.7	—	—	—	—	—	—	—	—	≤ 9.14E+30	—	—	—	—	—	—	—	—
DZ Cha <sup>20</sup>	LMS	150 ± 8	T <sup>25</sup>	70	15.0	450.0	9.103	8.506	7.548	1.58E-05	—	—	—	—	≤ 1.60E+28	—	—	—	—	—	—	—	—
RX J1604.3-2130A <sup>1,21</sup>	LMS	158 ± 6	T <sup>25</sup>	30	3.2	31.6	8.777	8.558	8.528	—	—	—	1.10E-02	—	≤ 1.16E+31	—	—	—	—	—	—	—	—
RXJ1615.3-3255 <sup>2</sup>	LMS	154 ± 7	T <sup>34</sup>	160	6.2	30.8	8.709	8.17	7.673	—	—	—	6.31E-03	—	≤ 9.10E+30	—	—	—	—	—	—	—	—
RXJ1842.9-3532 <sup>2</sup>	LMS	146 ± 7	T <sup>25</sup>	30	2.9	29.2	8.246	7.61	6.794	—	—	—	1.00E-02	—	≤ 2.17E+31	—	—	—	—	—	—	—	—
DoAr44 <sup>2</sup>	LMS	158 ± 8	MSp <sup>36</sup>	—	31.6	474.0	8.089	7.739	6.938	1.20E-03	—	—	—	—	≤ 4.01E+30	—	—	—	—	—	—	—	—
IM Lup <sup>1</sup>	IMS	398 ± 25	1Sp <sup>37</sup>	—	39.8	1194.0	8.203	7.408	6.344	9.12E-04	—	—	8.32E-03	3.63E-03	≤ 1.73E+31	—	—	—	—	—	—	—	—
V1247 Ori <sup>1,2,22</sup>	LMS	128 ± 7	—	—	12.8	384.0	8.342	8.015	7.716	1.91E-03	—	—	—	—	≤ 3.30E+30	—	—	—	—	—	—	—	—
DN Tau <sup>1</sup>	LMS	145 ± 7	—	—	14.5	435.0	9.776	9.332	9.016	—	—	—	—	—	≤ 1.12E+31	—	—	—	—	—	—	—	—
GO Tau <sup>1</sup>	LMS	159 ± 8	—	—	31.8	477.0	8.679	7.96	6.973	—	—	—	1.74E-03	—	≤ 3.26E+30	—	—	—	—	—	—	—	—
DL Tau <sup>1</sup>	LMS	162 ± 12	—	—	32.4	486.0	6.262	5.527	4.913	6.31E-04	—	—	—	—	≤ 1.18E+31	—	—	—	—	—	—	—	—
MWC 480 <sup>1</sup>	IMS	159 ± 8	—	—	31.8	477.0	8.431	7.793	6.775	2.75E-03	—	—	—	—	≤ 6.72E+30	—	—	—	—	—	—	—	—
CI Tau <sup>1</sup>	IMS	101 ± 12	FD, rings <sup>38</sup>	20.2	303.0	5.531	4.779	3.706	—	—	—	—	1.00E-03	—	≤ 1.03E+31	—	—	—	—	—	—	—	—
HD163296 <sup>23</sup>	IMS	140 ± 8	FD, rings <sup>40</sup>	28.0	168.0	9.171	7.41	5.298	—	—	—	—	1.00E-03	—	≤ 4.52E+30	—	—	—	—	—	—	—	—
HL Tau <sup>24</sup>	LMS	134 ± 9	DD <sup>41</sup>	100	2.7	26.8	6.862	6.227	5.783	—	—	—	—	—	≤ 1.25E+32	—	—	—	—	—	—	—	—
DoAr 21 <sup>2</sup>	IMS	180 ± 12	—	—	36.0	540.0	7.758	7.57	7.159	3.31E-03	—	—	—	—	≤ 1.93E+31	—	—	—	—	—	—	—	—
TYC 4496-780-1 <sup>1</sup>	IMS	344 ± 13	—	—	34.4	1032.0	9.472	8.831	7.722	2.75E-02	—	—	—	—	≤ 1.21E+32	—	—	—	—	—	—	—	—
IRAS 04028+2948 <sup>1</sup>	IMS	151 ± 7	—	—	15.1	453.0	9.46	9.308	9.148	3.02E-04	—	—	—	—	≤ 3.39E+29	—	—	—	—	—	—	—	—
V1075 Tau <sup>1</sup>	LMS	149 ± 18	—	—	14.9	447.0	8.317	8.129	8.074	3.98E-03	—	—	—	—	≤ 9.46E+30	—	—	—	—	—	—	—	—
V397 Aur <sup>1</sup>	LMS	125 ± 6	—	—	12.5	375.0	8.960	8.802	8.734	2.09E-03	—	—	—	—	≤ 1.94E+30	—	—	—	—	—	—	—	—
V1207 Tau <sup>1</sup>	IMS	151 ± 8	—	—	30.2	453.0	7.996	7.895	7.829	3.31E-04	—	—	—	—	≤ 1.09E+30	—	—	—	—	—	—	—	—
HIP 77545 <sup>1</sup>	IMS	152 ± 7	—	—	30.4	456.0	7.429	7.294	7.261	9.12E-04	—	—	—	—	≤ 5.15E+30	—	—	—	—	—	—	—	—
HIP 79462 <sup>1</sup>	IMS	144 ± 8	—	—	28.8	432.0	7.904	7.785	7.728	8.32E-04	—	—	—	—	≤ 2.71E+30	—	—	—	—	—	—	—	—
HIP 80088 <sup>1</sup>	LMS	160 ± 13	DD <sup>34</sup>	190	16.0	480.0	8.318	8.148	8.058	2.75E-03	—	—	—	—	≤ 7.55E+30	—	—	—	—	—	—	—	—

Table 1. Stars with protoplanetary disks imaged within 0".25 with sufficient sensitivity to detect a 0.1 L<sub>⊙</sub> companion.

Note— [1]Uyama et al. 2017, [2]Wilson et al. 2016, [3]Cugno et al. 2019, [4]Quanz et al. 2013, [5]Sissa et al. 2018, [6]Currie et al. 2017, [7]Follette et al. 2017, [8]Grady et al. 2013, [9]Reggiani et al. 2018, [10]Maire et al. 2017, [11]Gratton et al. 2019, [12]Luigi et al. 2018, [13]Mawet et al. 2017, [14]Christians et al. 2018, [15]Keppler et al. 2018, [16]Haffert et al. 2019, [17]Kraus & Ireland 2012, [18]Sallum et al. 2015, [19]Cieza et al. 2013, [20]Canovas et al. 2018, [21]Canovas et al. 2017, [22]Kraus et al. 2013, [23]Guidi et al. 2018, [24]Testi et al. 2015, [25]Espillat et al. 2014b, [26]Tang et al. 2017, [27]Akiyama et al. 2016, [28]Grady et al. 2001, [29]Follette et al. 2017, [30]Currie et al. 2013, [31]Muto et al. 2012, [32]Gratton et al. 2012, [33]Maffei et al. 1998, [34]van der Marel et al. 2016, [35]Currie & Sicilia-Agular 2011, [36]Avenhaus et al. 2018, [37]Dong et al. 2018b, [38]Clarke et al. 2016, [40]ALMA Partnership et al. 2015, [41]Jensen et al. 2009

<sup>a</sup> Transition disks are indicated by T, debris disks by DD, and full disks by FD. One-armed, two-armed, and multiarmed spirals are indicated by 1Sp, 2Sp, and MSp respectively. Disks with imaged ring structure are indicated by "Rings".

Star	Mass	dist	Stellar Magnitude			Contrast			$\lambda L_\lambda$ (erg s <sup>-1</sup> )		
			pc	H	K <sub>s</sub>	L	$\Delta$ H	$\Delta$ K <sub>s</sub>	$\Delta$ L	H	K <sub>s</sub>
HD 142527 <sup>1</sup>	IMS	157 ± 1	5.715	4.980	4.280	–	–	–	4.39E+32	2.35E+32	8.12E+31
LkCa 15b <sup>2,3,4</sup>	LMS	159 ± 8	8.600	8.163	7.49	5.25E-03	3.98E-03	1.00E-02	1.10E+31	6.16E+30	7.72E+30
LkCa 15c <sup>4</sup>	LMS	159 ± 8	8.600	8.163	7.49	5.25E-03	3.98E-03	1.00E-02	9.70E+30	6.16E+30	–
PDS 70b <sup>5,6</sup>	LMS	113 ± 5	8.823	8.542	8.026	–	6.31E-04	1.74E-03	–	3.51E+29	4.18E+29
PDS 70c <sup>6</sup>	LMS	113 ± 5	8.823	8.542	8.026	–	3.02E-04	2.29E-03	–	1.68E+29	5.46E+29

**Table 2.** Stars with accreting companions imaged.

NOTE—[1]Christiaens et al. 2018, [2]Uyama et al. 2017, [3]Kraus & Ireland 2012, [4]Sallum et al. 2015, [5]Keppler et al. 2018, [6]Haffert et al. 2019

Star	a	M	$\dot{M}$	$L/L_{\odot}$
	(au)	( $M_J$ )	( $M_J^2 \text{ yr}^{-1}$ )	
HD 142527B <sup>1</sup>	$22^{+19}_{-11}$	$270^{+170}_{-150}$	$10^{-2}$ [4]	0.6
LkCa 15b <sup>2</sup>	$14.7 \pm 2.1$	$\leq 10$	$10^{-5}$	$\sim 10^{-3}$
LkCa 15c <sup>2</sup>	$18.6 \pm 2.5$	$\leq 10$	$10^{-5}$	$\sim 10^{-3}$
PDS 70b <sup>3</sup>	$20.6 \pm 1.2$	4–17	$0.3 - 9 \times 10^{-7}$	$\sim 10^{-4}$
PDS 70c <sup>3</sup>	$34.5 \pm 2.0$	4–12	$0.15 - 6 \times 10^{-7}$	$\sim 10^{-4}$

**Table 3.** Companion data

NOTE—[1]Christiaens et al. 2018, [2] Sallum et al. 2015, [3] Haffert et al. 2019, [4]  $\dot{M}$  is estimated by assuming that luminosity of the companion object is dominated by the accretion luminosity and that the radius of the companion is  $1.5R_J$ .

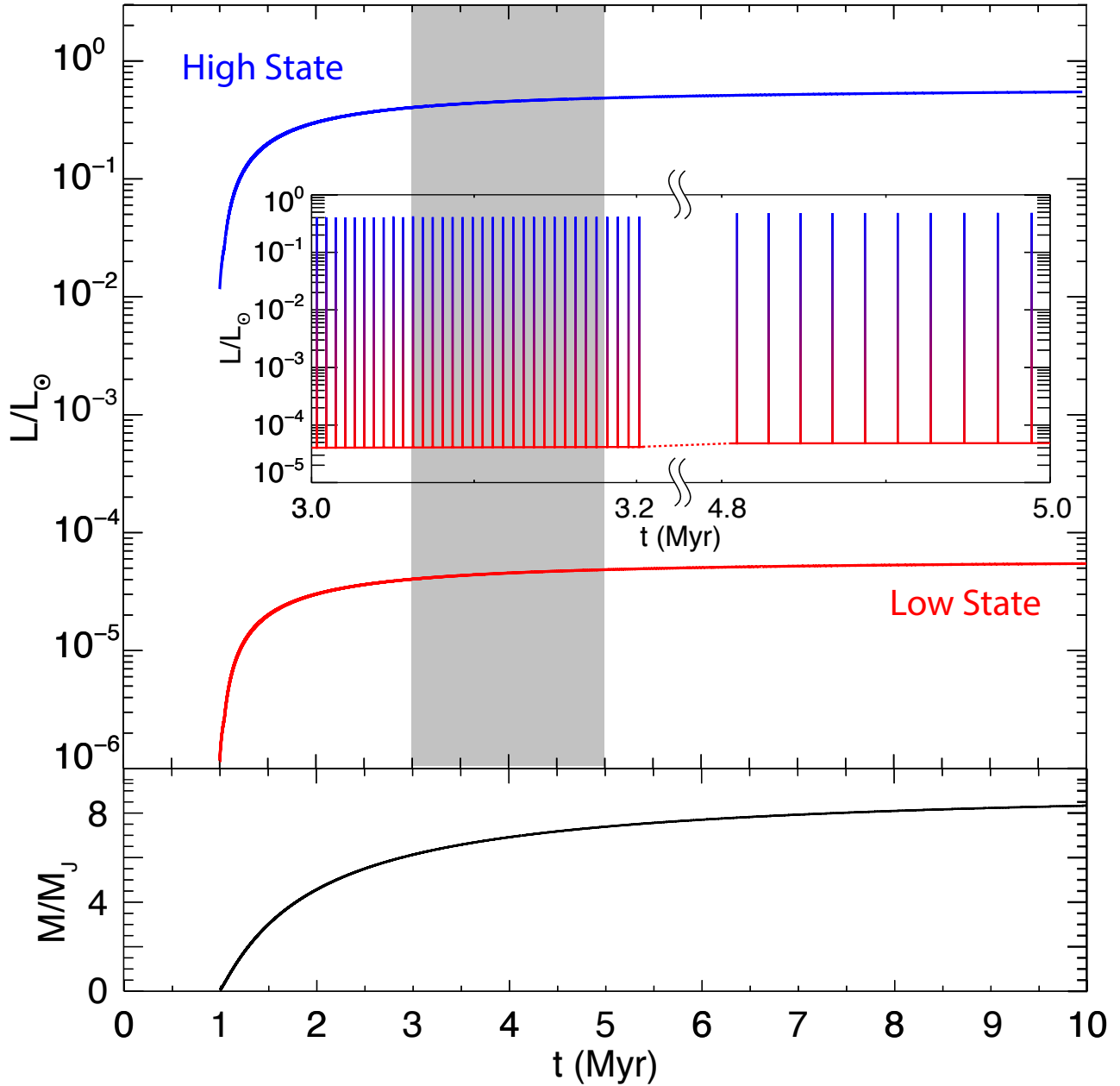


**Figure 1.** Accretion luminosity (upper panel) and planetary mass (lower panel) as a function of time. The accretion luminosity increases with planetary mass and alternates between quiescence (red curve) and outburst (blue curve). The inset shows an enlarged version of the shaded region of the plot. When the planet mass is low and the circumstellar disk accretion rate is high, outbursts are more frequent as the circumplanetary disk grows in mass to  $0.1 M_p$  more frequently. However the potential well is not as deep and the accreted mass is lower, so the luminosity of the accretion is lower. As the planet grows in mass and the circumstellar disk accretion rate declines, the outbursts become less frequent but more intense. In the model shown, the planet mass grows to  $\sim 8 M_J$  in 5 Myr and continues to grow until the circumstellar disk ceases to feed the circumplanetary disk and the circumplanetary disk empties all of its mass onto the central object.

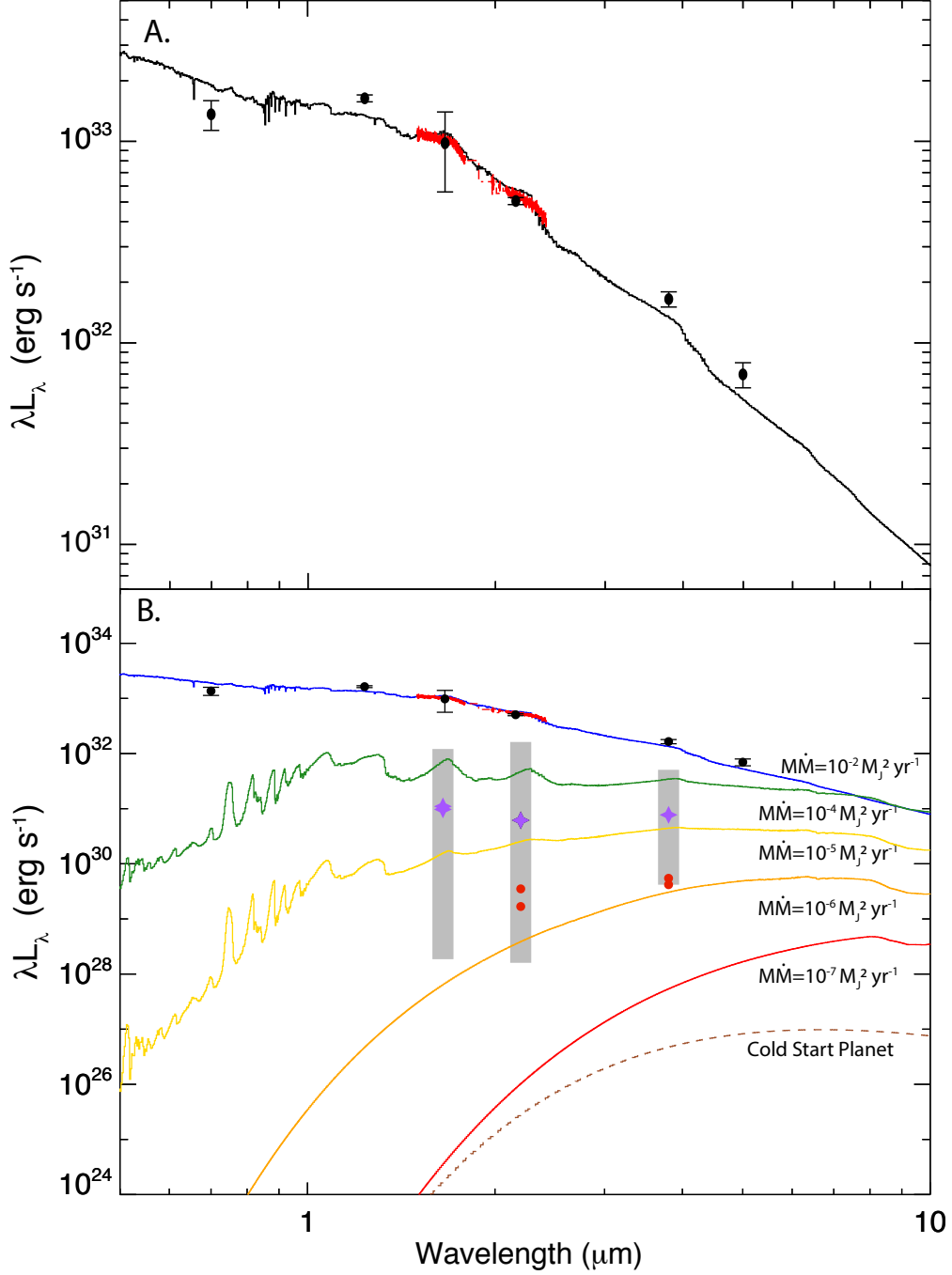


**Figure 2.** Photometry of the companion orbiting HD142527 and models of active circumplanetary disks. The companion photometry is corrected for circumplanetary disk inclination and reddening following [Zhu \(2015\)](#) assuming an inclination of  $70^\circ$ ,  $A_J = 1.6$  and  $\alpha = 1.7$ . With these parameters, the photometry of the companion is well fit by a model of an active disk with  $\dot{M} = 10^{-2} M_J^2 \text{ yr}^{-1}$ ,  $R_{in} = 1.5 R_J$ , and  $R_{out} = 15 R_J$  (Panel A). In Panel B, we replot the companion photometry as well as the photometry of the candidate planets orbiting LkCa 15 (purple stars) and PDS 70 (red circles). The range of observational limits from the literature are shown as vertical gray bars. We also plot the SED of an accreting circumplanetary disk for four additional accretion rates as well as the spectrum of a 550 K blackbody representing a cold-start 1 Myr old  $1 M_J$  planet. Previous observations are not sensitive enough to have detected a gas giant planet with a quiescent disk ( $\dot{M} < 10^{-6} M_J^2 \text{ yr}^{-1}$ ).